Electronic Supplementary Information (ESI)

Synthetic methods for key precursors of biologically active dimethylsulfoxide ruthenium complexes

Sreshtha Nayek,[a] Rodrigo S. Correa,*[a,b] Ehsan Ezzatpour Ghadim,*[a,d] Juliusz A. Wolny,[c] Volker Schünemann,[c] Rafael Cavalieri Marchi,*[a,d] and Peter J. Sadler*[a]

*Corresponding author

[a] *Department of Chemistry, University of Warwick, Gibbet Hill Road, Coventry CV4 7AL, United Kingdom, Ehsan.Ezzatpour-Ghadim.3@warwick.ac.uk, P.J.Sadler@warwick.ac.uk*

[b] *Department of Chemistry, Federal University of Ouro Preto, Ouro Preto 35402-136, Brazil, rodrigocorrea@ufop.edu.br*

[c] *Department of Physics, University of Kaiserslautern, Erwin-Schrödinger-Str. 46, 67663 Kaiserslautern, Germany*

[d] *School of Engineering, University of Warwick, Gibbet Hill Road, Coventry CV4 7AL, United Kingdom, Rafael.Cavavelieri-Marchi@warwick.ac.uk*

Contents

	Experimental Section	S4
	Methods and Characterisation	S7
Scheme 1.	Summary of reactions of $RuCl_3.3H_2O$ with neat DMSO or with the addition of conc. HCl for various times T1 and T2	S4
Table S1.	Details of reaction procedures **H1-4**, **MW1-5** and **S1**, observations and products formed	S11
Table S2.	Summary of the crystal data and structure refinement parameters for complexes **1–4**	S12
Table S3.	Selected bond distances (Å) for complexes **1-4**	S14
Table S4.	Selected bond angles in degrees for complex **1** at 100K and 250 K, and polymorph **2'**	S15
Table S5.	Selected bond angles in degrees for complexes **2-4**	S16
Table S6.	Differences in the unit cell parameters in previously reported monoclinic and orthorhombic forms of complex **2**	S17
Table S7.	TD-DFT calculated UV-vis spectra wavelengths, extinction coefficients and their transition type	S18
Table S8.	Observed cathodic and anodic peaks for complexes **1-4** in the cyclic voltammetry (CV)	S18
Figure S1.	HRMS data for complex **1-3**	S19
Figure S2.	HRMS and ^{1}H-NMR (500 MHz) spectrum for complex **4**	S19
Figure S3.	Comparison between experimental (black) and theoretical (red) powder X-ray diffraction (PXRD) patterns of complexes **1-4** obtained through the different synthetic methods	S20
Figure S4.	Single crystal X-ray diffraction (SCXRD) structures of complex **1** obtained at 250 K and 100 K, complex **2** and complex **2'** (polymorph), complex **3** and complex **4**	S22
Figure S5.	Differential scanning calorimetry (DSC) of **1** confirming a phase transition in the range of 163-133 K and differences in the crystal packing view of complex **1** along *a*-axis at 298 K and at 100K.	S25
Figure S6.	Perspective view showing the conformational difference between the two molecules A and B of polymorph **2'**	S27

Figure S7.	DFT calculated structures of complex **4** Ru(IV)-(IV) and one electron reduced **4** Ru(III)-(IV)	S28
Figure S8.	UV-vis spectra of complexes **1-4** in acetonitrile	S29
Figure S9.	Cyclic voltammograms of complexes **1-4** in acetonitrile solution at a scan rate of 100 mV s^{-1}	S29
Figure S10.	400 MHz ^{1}H-NMR spectrum of complex **4** in D_2O, 10 min and 24 h after dissolution at 293 K	S30
Figure S11.	UV-vis spectra of complex **4** on reaction with 0.5 mol and 2 equiv of ferrocene in acetonitrile, monitored for 30 mins	S31
Figure S12.	Comparison of ferrocene, ferrocenium, complex **4** and reduced **4** UV-vis spectra in the region between 450 nm to 800 nm	S31
Figure S13.	Plots of ln (A/A_0) vs time of reaction between **4** and 0.5, 1 and 2 mol equiv of Fc	S32
Figure S14.	Comparison between ^{1}H-NMR spectrum (500 MHz, acetonitrile-d_3) of complex **4** before and after 30 min of ferrocene addition	S33
Figure S15.	Positive-ion HRMS scan for product obtained from reaction between complex **4** and ferrocene (1 mol equiv) in acetonitrile after 15 min of reaction	S34
Figure S16.	Calculated spin density in one-electron reduced **4**	S35
	References	S36

S1. Experimental Section

S1.1. Chemicals

$RuCl_3.3H_2O$ was purchased from Precious Metals Online. DMSO (analytical reagent grade) and HCl (37%) was obtained from Fischer Chemical. Acetone (reagent grade), acetonitrile (HPLC grade), ferrocene and deuterated acetonitrile, water and methanol were purchased from Sigma-Aldrich. Ethanol absolute was obtained from VWR Chemicals. All reagents were used without further purification.

S1.2. Syntheses of Complexes

All synthetic procedures were repeated at least three times with reproducible results. The reactions are summarised below:

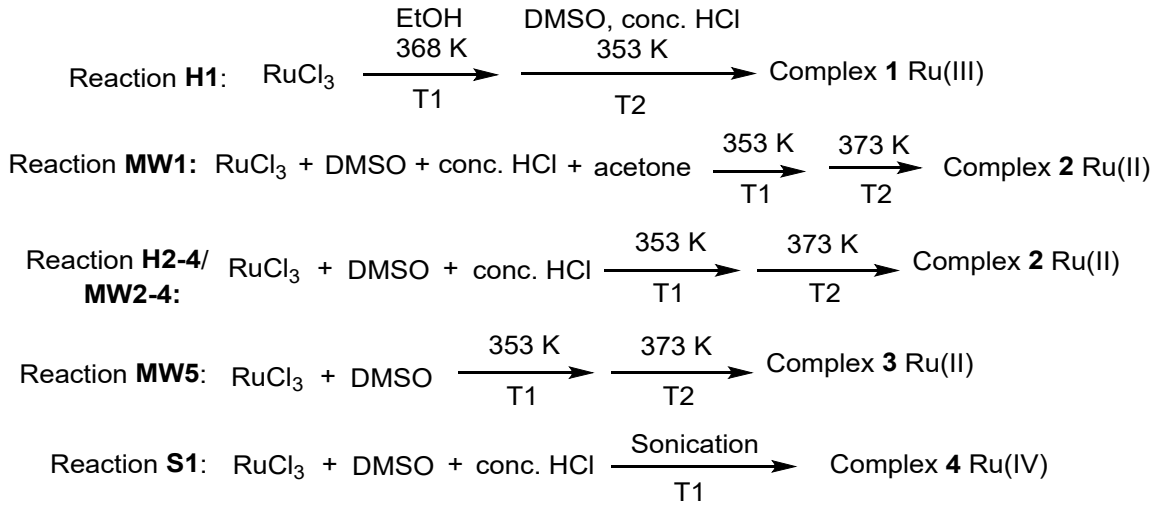

Scheme 1: Summary of reactions of $RuCl_3.3H_2O$ with neat DMSO or with addition of conc. HCl for various times, T1 and T2. **H** = hotplate, **MW =** microwave-assisted and **S** = ultrasound bath-assisted syntheses. For **H** reactions, T1 = 20 min or 3 h, T2 = 30 – 90 min. For **MW** reactions, T1 = 5 min, T2 = 10 – 20 min. For **S1**, T1 = 40 min. Details of reaction times are described below, and observations are in **Table S1**.

S1.2.1. Hotplate Heating: Reactions ***H1-H4*** were carried out using an IKA-Werke RCT basic hotplate magnetic stirrer. The hotplate was allowed to reach the desired temperature before commencing time measurement. Reactions were stirred at 1200-1300 rpm.

Reaction *H1*: This reaction procedure followed that reported by Alessio *et al.*[1] $RuCl_3.3H_2O$ (250 mg, 0.96 mmol) was suspended in ethanol (7.5 mL, 128.61 mmol) and refluxed for 3 h at 368 K. The obtained dark green solution was filtered and concentrated to ~ 1 mL under reduced pressure. Next, HCl (37% w/w, 250 μL, 8.04 mmol) and DMSO (500 μL, 7.04 mmol) were added and allowed to react at 353 K for 15 min after which the solution changed colour to bright orange. After the reaction mixture cooled to room temperature (293-295 K), 2.5 mL of acetone was added and left overnight. Needle-like orange crystals of complex **1** obtained in 48 h were filtered and washed with cold acetone and diethyl ether. Yield 65 ± 5%.

Reactions *H2-H4*: In a round-bottom flask, $RuCl_3.3H_2O$ (250 mg, 0.96 mmol), DMSO (1.16 mL, 16.33 mmol) and HCl (37% w/w, 166 μL, 5.34 mmol) were added and the solution was stirred at 353 K for 20 min and then the temperature was raised to 373 K for 60 min (***H2***), 30 min (***H3***) or 90 min (***H4***) to form a clear orange solution. Each reaction was left to cool down to room temperature (293 K), followed by the addition of 5 mL acetone. A small amount (*ca.* 250 μL) of diethyl ether was added to increase the rate of crystal formation. Orange block-like crystals (yield 36 ± 4%) and yellow square-shaped crystals (yield 20 ± 3%) of complex **2** were formed for ***H2*** and ***H3,*** respectively, within 24 h. These crystals were filtered off and washed with diethyl ether to remove excess DMSO. In the case of ***H4***, after acetone addition, a precipitate formed immediately and was readily filtrated off. The clear orange filtrate was kept in a vial with the lid open for crystallisation at room temperature (293-295 K). Orange coloured elongated hexagonal-shaped single crystals of complex **2'** (polymorph of **2**) were formed the next day (yield 12 ± 1%).

S1.2.2. Microwave-Assisted Syntheses: Reactions (***MW1-MW5***) were carried out in G-30 (30 mL) vials using the Anton Paar Monowave 200 reactor with 850 W power, with a frequency of 2.45 GHz and a wavelength of 12.24 cm.

Reactions *MW1-MW5*: In a G30 glass vial, $RuCl_3.3H_2O$ (250 mg, 0.956 mmol), DMSO (1.16 mL, 16.33 mmol), and HCl (37% w/w, 166 μL, 5.34 mmol) were added. Acetone (5 mL) was added in reaction in the beginning of the reaction ***MW1*,** and HCl was not added in ***MW5***. Each reaction mixture (***MW1-MW5***) was stirred at 500 rpm. The temperature was increased from room temperature (293 K) to 353 K at a steady controlled rate of 285 K/min and then from 353 K to 373 K at a controlled rate. Solutions were heated at these two temperatures for different

lengths of time. After reaction completion, all reaction mixtures were allowed to cool down to 343 K at a controlled rate in the microwave reactor and then left outside the reactor to cool down to room temperature (293-295 K). Afterwards, 5 mL of acetone was added to the solutions ***MW2-MW5*****.** In all reaction conditions (***MW1-MW5*****),** small amounts of diethyl ether (*ca.* 250 μL) were added to increase the rate of crystal formation and were left in an open vial at ambient temperature (293-295 K) for crystallisation. The crystals were filtered off and washed with diethyl ether. The variations in heating durations, observations and yields for individual reactions are given below.

MW1**:** The mixture was reacted at 353 K for 5 min and 373 K for 15 min. After 3-4 days at 293 K, a mixture of orange hexagonal and a few needle-like crystals of complex **2** was observed. Yield 47 ± 3%.

MW2**:** The reaction mixture had the same heating profile as ***MW1***, i.e., the mixture was reacted at 353 K for 5 min and 373 K for 15 min. A clear orange solution was left for crystallisation and hexagonal orange crystals of complex **2** were formed in 3-4 days. Yield 32 ± 5%.

MW3**:** The reaction mixture was reacted at 353 K for 5 min and 373 K for 10 min. Crystal formation took 3 weeks and very few yellow crystals of complex **2** were formed. Yield 12 ± 3%.

MW4**:** The reaction mixture was reacted at 353 K for 5 min and 373 K for 20 min. A clear orange solution was obtained which on crystallisation formed yellow crystals of complex **2** in 3-4 days. Yield 62 ± 8%.

MW5**:** The mixture was heated at 353 K for 5 min and 373 K for 15 min. The solution obtained was dark brownish in colour, in contrast to the clear orange solution in ***MW1-MW4***. Crystal formation took a week, and the orange crystal obtained was of complex **3**. Yield 68 ± 7%.

S1.2.3. Sonication-Assisted Synthesis: Reaction ***S1*** was performed using a Branson 2510 ultrasound bath with a frequency of 40 kHz and a maximum input power of 130 W.

Reaction *S1*: $RuCl_3.3H_2O$ (250 mg, 0.956 mmol) in DMSO (1.16 mL, 16.33 mmol) and HCl (37% w/w, 166 μL, 5.34 mmol) were taken in a 25 mL glass vial and sonicated for 40 min with maximum power of 130 W. Once the sonication stopped, 5 mL of acetone was then added to the reaction mixture and kept at room temperature (293-295 K) in a vial with lid open for three weeks for crystal formation. The dark brown crystals of complex **4** were filtered and washed with diethyl ether to remove excess DMSO. Yield 62 ± 5%.

S1.3. Methods and characterisation

S1.3.1. High-resolution mass spectrometry

High-resolution mass spectrometry (HRMS) was recorded with a Bruker maXis plus QTOF in -ve mode for complex **1** and in +ve mode for complexes **2-4**. Complexes were dissolved in acetonitrile.

S1.3.1. ^{1}H-NMR

Proton spectra (^{1}H-NMR) were recorded at 298 K on an Avance HD 400 MHz and an Avance HD 500 MHz (^{1}H frequencies) with complex solutions at 6 mg/mL. Proton spectra were recorded with standard pulse sequences. ^{1}H chemical shifts were referenced to residual solvent peaks: CD_3OD (3.31 ppm), CD_3CN (1.94 ppm). Data were processed in MestreNova (Mestrelab, Spain).

S1.3.2. UV-vis

UV-visible absorption spectra were recorded on a Varian Cary 300 UV-visible spectrometer in a quartz 3 mL cuvette with 1-cm width and using the solvent to measure the baseline. The spectral width was 200–800 nm and the bandwidth was 1.0 nm. The absorption spectra of complexes **1-4** were recorded in acetonitrile at concentrations of 0.2 mM, 1.6 mM, 3.3 mM and 0.07 mM, respectively.

S1.3.3. Cyclic voltammetry

Electrochemical measurements were made using a CH Instruments model Electrochemical Analyzer. Cyclic voltammograms were carried out using 0.1 M NBu_4PF_6 as supporting electrolyte and 1.0 mM of complexes **1-4** in acetonitrile at 298 K under N_2 at a scan rate of 100 mV/s. A platinum disc working electrode, a platinum wire counter electrode, and a reference electrode AgCl/Ag, separated from the test solution by a salt bridge containing the

solvent/supporting electrolyte were used in the experiments. With this experimental setup, the ferrocene/ferrocenium couple appeared at 0.1 V with $\Delta E_p = 68$ mV.

S1.3.4. X-ray crystal structures

Single-crystal X-ray diffraction (SCXRD) data were collected on an Oxford Diffraction Synergy-S equipped with a large theta coverage detector HyPix-Arc 100° and a four-circle system. All measurements were carried out at 100 K and additionally at 253 K for **1** and 293 K for **2'**, using Mo [Kα = 0.71073 Å] or Cu [Kα = 1.54060 Å] as the radiation source. CrysAlisPro was used for complete data collection and processing.[2] The crystal structures were solved by direct methods using SHELXS and refined by full-matrix least squares against F^2 using SHELXL 97.[3] Anisotropic displacement parameters were used for all non-H atoms. Meanwhile, H-atoms were added at calculated positions and refined using a riding model, considering Uiso(H) = 1.5Ueq(Cmethyl). The Mercury 2024.2.0 program[4] was used for the analysis of intra- and intermolecular contacts and to generate the structure representation.

X-ray crystallographic data for complexes have been deposited in the Cambridge Crystallographic Data Centre (CCDC) under the accession numbers 2483730 (**1** at 100K), 2483731 (**1** at 250K), 2483732 (**2**), 2483733 (**2'**), 2483734 (**3**), 2483735 (**4**). X-ray crystallographic data in CIF format are available from the Cambridge Crystallographic Data Centre (http://www.ccdc.cam.ac.uk/). The Cambridge Structural Database (CSD) (CSD version 6.00 updated in April 2025) was used to access the reported crystal structures for comparison: For complex **1** [CSD codes: JIMKAR and JIMKAR01, complex **2** [CSD codes: CDMSOR-CDMSOR06] and complex **3** (CSD codes: KACNOR-KACNOR06)].

S1.3.5. Powder X-ray diffraction (PXRD)

PXRD experiments were conducted on Anton Paar XRDynamic 500 equipped with a Primux 3000 X-ray tube giving Co $K\alpha_{1,2}$ radiation (λ = 1.7902 Å) and a Pixos 2000 1D detector. The crystals were ground powders and were mounted on the Anton Paar TTK 600 stage. Each scan was recorded with a step size of 0.01° and within an angular range of 5.0–60.0° (2θ). Simulated PXRD pattern based on the SCXRD data was generated with the program Mercury[4].

S1.3.6. Hydrolysis complex 4 followed by UV-vis and NMR

Crystals of **4** were ground into fine powder, dissolved in milli-Q water, and the concentration was quickly adjusted to 0.1 mM. This procedure was done due to difficulties of solubilisation of the whole crystal in water. UV-vis absorption spectra were recorded on a Varian Cary 300

UV-visible spectrometer every 1 min for a period of 60 min with constant stirring using a quartz 3 mL cuvette with a 1-cm width. Similarly, the process was studied by ^{1}H NMR spectroscopy with *ca.* 10 mM of complex **4**.

S1.3.7. Reaction between complex 4 and ferrocene

Complex **4** was dissolved in acetonitrile (*ca.* 0.1 mM, concentration determined from absorption spectra, ε_{464nm}= 9889 cm^{-1} L mol^{-1}) with ferrocene (0.5, 1 and 2 mol equiv) and the reactions were monitored by UV-vis spectroscopy every 1 min for a period of 60 min with constant stirring using a quartz 3 mL cuvette with 1-cm width. The reaction was also studied by ^{1}H NMR spectroscopy (**4** = 10 mM, Fc = 2 mol equiv).

S1.3.8. DFT Modelling

Complex **4** was modelled using the B3LYP fuctional[5] and def2QZVP basis set[6] with the Grimme's D3 dispersion correction.[7] The starting geometry was taken from the X-ray data and optimised. The one-electron reduced Ru(IV)-Ru(III) complex was also optimised on the basis of the optimised structure of **4** assuming the charge of -1 and a doublet ground state. Additionally, the analogue with DMSO ligand replaced by MeCN, [(Ru(IV)Cl_3(MeCN)$_2$)$_2$(μ-O)] (**4a**) was modelled. The electronic absorption spectra of complex **4,** reduced **4**, complex **4a**, reduced **4a** were derived by means of TD-DFT, for six singlets and six triplets in the Ru(IV)-Ru(IV) forms and six allowed doublet to doublet transitions for the reduced forms.

S1.4. Characterisation of complexes

*Complex **1***: ESI-MS: Obs. 243.7778, calc. for [$RuCl_4$]$^-$ 243.7881 m/z, error = 1.2 ppm (**Figure S1**). ^{1}H NMR (500 MHz, CD_3OD): δ = -14.48 (s, 12 H, Ru(III)-DMSO). The peak is broad and shifted upfield due to the paramagnetism of Ru(III) (same as reported[8]). Elemental analysis (%) Calc. for $C_8H_{25}Cl_4O_4RuS_4$: C, 17.27; H, 4.53. Found: C, 17.18; H, 4.51.

*Complex **2***: ESI-MS: Obs. 508.8857, calc. for [M+Na]$^+$ 508.8854 m/z, error = 0.58 ppm (**Figure S1**). ^{1}H NMR (400 MHz, CD_3CN): δ = 3.39 (s, 6 H, DMSO), 3.38 (s, 6 H, DMSO), 3.37 (s, 6 H, DMSO). Upon dissolution, complex **2** shows a fast DMSO labilisation with each signal integrating to 6 H while a free DMSO is observed at 2.58 ppm in accordance with other published data.[9,10] Elemental analysis (%) Calc. for $C_8H_{24}Cl_2O_4RuS_4$: C, 19.83; H, 4.99. Found: C, 19.64; H, 4.96.

*Complex **3***: ESI-MS: Obs. 430.8736, calc. for $[M\text{-}DMSO+Na]^+$ 430.8716 m/z, error = 4.6 ppm (**Figure S1**). ^1H NMR (400 MHz, CD_3CN) s): δ = 3.23 (s, 24H, 4 DMSO). Complex **3** is highly symmetrical and NMR in accordance with other published data.[9,10] Elemental analysis (%) Calc. for $C_8H_{24}Cl_2O_4RuS_4$: C, 19.83; H, 4.99. Found: C, 19.67; H, 5.00.

*Complex **4***: ESI-MS: obs. 766.6824, calc. for $[M+Na]^+$ 766.6585 m/z, error = 24 ppm. ^1H NMR (500 MHz, CD_3CN): δ = 3.0 (s, 12 H, 2 DMSO), 2.5 (s, 12 H, 2 DMSO) (**Figure S2**). Elemental analysis (%) Calc. for $C_8H_{24}Cl_6O_5Ru_2S_4$: C, 12.93; H, 3.25. Found: C, 13.04; H, 3.30.

Table S1. Details of reaction procedures **H1-4** (thermal hotplate), **MW1-5** (microwave) and **S1** (ultrasound), observations and products formed. Times T1 and T2 are indicated in **Scheme 1**. For **H1**, T1 = 368 K and T2 = 353 K. For **H2-4**/ **MW1-5**, T1 = 353 K and T2 = 373 K.

Method	T1	T2	Observation	Comments and Yield	Observation of Crystal	Chemical Structure (Complex no.)
H1	3 h	15 min	Deep orange solution	65%	Needle-like orange crystals in 2 days	$[(DMSO)_2H]$ *trans*-$RuCl_4(DMSO)_2]$ (**1**)
H2	20 min	60 min	Clear orange solution	36%	Orange crystals in 24h	*cis*-$[RuCl_2(DMSO)_4]$ (**2**)
H3	20 min	30 min	Clear orange solution	20%	Yellow crystals in a block shape in 24h	*cis*-$[RuCl_2(DMSO)_4]$ (**2**)
H4	20 min	90 min	Clear orange solution	12%	Orange elongated hexagonal crystals in 24h	*cis*-$[RuCl_2(DMSO)_4]$ (**2'**) (Monoclinic IV polymorph)
MW1	5 min	15 min	Clear orange solution	(Acetone added before) 47%	Orange hexagonal and a few needle-like crystals in 3-4 days	*cis*-$[RuCl_2(DMSO)_4]$ (**2**)
MW2	5 min	15 min	Clear orange solution	32%	Hexagonal orange crystals after 3-4 days	*cis*-$[RuCl_2(DMSO)_4]$ (**2**)
MW3	5 min	10 min	Clear orange solution	12%	Yellow coloured crystal formation after 3 weeks	*cis*-$[RuCl_2(DMSO)_4]$ (**2**)
MW4	5 min	20 min	Clear orange solution	62%	Yellow crystals after 3-4 days	*cis*-$[RuCl_2(DMSO)_4]$ (**2**)
MW5	5 min	15 min	Dark brownish solution	(No HCl added) 68%	Orange crystals in 1 week	*trans*-$[RuCl_2(DMSO)_4]$ (**3**)
S1	40 min		Dark red solution	62%	Dark brown crystal formation in 3 weeks	$[(cis\text{-}RuCl_3(DMSO)_2)_2(\mu\text{-}O)]$ (**4**)

Table S2. Summary of the crystal data and structure refinement parameters for complexes **1–4**

Complex	**1 (100 K)**	**1 (250 K)**	**2**	**2'** (Polymorph)	**3**	**4**
Empirical formula	$C_8H_{25}Cl_4O_4RuS_4$	$C_8H_{25}Cl_4O_4RuS_4$	$C_8H_{24}Cl_2O_4RuS_4$	$C_8H_{24}Cl_2O_4RuS_4$	$C_8H_{24}Cl_2O_4RuS_4$	$[C_8H_{24}Cl_6O_5Ru_2S_4]$ ½ H_2O
Formula weight	556.39	556.39	484.48	484.48	495.47	752.36
Temperature/K	100(10)	250(2)	100(10)	293(2)	100(10)	100(2)
Crystal system	Triclinic	Monoclinic	Orthorhombic	Monoclinic	Tetragonal	Orthorhombic
Space group	*P*-1	*P*2/*n*	*Pccn*	$P2_1$	*I*4/*m*	*Ibca*
a/Å	9.1740(3)	9.25130(10)	10.80843(17)	8.3204(4)	9.0653(2)	13.5694(4)
b/Å	13.8779(4)	16.4925(2)	28.1464(4)	27.6671(9)	9.0653(2)	18.7428(6)
c/Å	16.4160(3)	14.0096(2)	11.62787(18)	8.5526(5)	11.0288(2)	20.3110(6)
α/°	90.864(2)	90	90	90	90	90
β/°	90.504(2)	100.8040(10)	90	117.043(7)	90	90
γ/°	100.618(2)	90	90	90	90	90
Volume/Å^3	2053.85(10)	2099.65(5)	3537.41(9)	1753.56(17)	906.34(4)	5165.7(3)
Z	2	4	8	4	2	8
ρ_{calc}g/cm^3	1.799	1.760	1.819	1.835	1.816	1.935
μ/mm^{-1}	14.865	14.534	1.665	1.679	1.671	2.131
F(000)	1137.9	1124	1968.0	984	503.0	2968
Crystal size/mm^3	0.2 × 0.15 × 0.13	0.25 x 0.19 x 0.13	0.16 × 0.15 × 0.13	0.29 x 0.11 x 0.10	0.17 × 0.15 × 0.12	0.15 x 0.10 x 0.05
Radiation	Cu Kα (λ =1.54184)	Mo Kα (λ = 0.71073)	Mo Kα (λ = 0.71073)	Mo Kα (λ = 0.71073)	Mo Kα (λ = 0.71073)	Mo Kα (λ = 0.71073)
2Θ range for data collection/°	5.38 to 147.6	2.679 to 73.553	5.346 to 61.55	2.674 to 29.532	5.818 to 59.264	2.731 to 29.587
Index ranges	-11 ≤ h ≤ 11, -17 ≤ k ≤ 17, -20 ≤ l ≤ 20	-11 ≤ h ≤ 11, -19 ≤ k ≤ 20, -17 ≤ l ≤ 16	-13 ≤ h ≤ 15, -39 ≤ k ≤ 35, -13 ≤ l ≤ 16	-10≤h≤11, -36≤k≤35, -10≤l≤11	-12 ≤ h ≤ 11, -11 ≤ k ≤ 11, -13 ≤ l ≤ 14	-18≤h≤16, -22≤k≤25, -26≤l≤24
Reflections collected	13868	16733	37166	9625	5058	2319
Independent reflections	13868 [R_{sigma} = 0.0415]	4133 [R_{int} = 0.0410]	4651 [R_{int} = 0.0291, R_{sigma} = 0.0169]	6817 [R_{int} = 0.0348]	621 [R_{int} = 0.0232, R_{sigma} = 0.0153]	3059 [R_{int} = 0.0278]
Data/restraints/parameters	13868/0/398	4133 / 0 / 225	4651 / 0 / 180	6817 / 1 / 359	621 / 0 / 35	3059 / 6 / 158
Goodness-of-	0.993	1.040	1.060	1.023	1.143	1.047

fit on F^2						
Final R indexes [$I>=2\sigma(I)$]	R_1 = 0.0439, wR_2 = 0.1180	R_1 = 0.0274, wR_2 = 0.0689	R_1 = 0.0194, wR_2 = 0.0435	R_1 = 0.0321, wR_2 = 0.0699	R_1 = 0.0244, wR_2 = 0.0656	R_1 = 0.0343, wR_2 = 0.1006
Final R indexes [all data]	R_1 = 0.0483, wR_2 = 0.1240	R_1 = 0.0300, wR_2 = 0.0708	R_1 = 0.0223, wR_2 = 0.0445	R_1 = 0.0377, wR_2 = 0.0721	R_1 = 0.0258, wR_2 = 0.0664	R_1 = 0.0432, wR_2 = 0.1063
Largest diff. peak/hole / e $Å^{-3}$	1.80/-1.20	0.437/-0.591	1.02/-0.54	0.711/ -1.125	0.69/-0.92	1.506/ -0.481

Table S3. Selected bond distances in Å for complexes **1**-**4**. Atoms are labelled in **Figure S4** for clarity.

	Complex 1 (100 K)		Complex 1 (250 K)		Complex 2	
Ru-S	Ru1-S1	2.3372(7)	Ru1-S1	2.3454(5)	Ru1-S1	2.2481(4)
	Ru1-S2	2.3427(7)	Ru2-S2	2.3484(5)	Ru1-S2	2.2700(4)
	Ru2-S3	2.3417(7)			Ru1-S3	2.2716(4)
	Ru2-S4	2.3408(7)				
Ru-Cl	Ru1-Cl3	2.3429(6)	Ru1-Cl1	2.3444(9)	Ru1-Cl2	2.43354(4)
	Ru1-Cl4	2.3544(6)	Ru1-Cl3	2.3532(9)	Ru1-Cl1	2.4142(4)
	Ru1-Cl15	2.3553(7)	Ru1-Cl2	2.3542(6)		
	Ru1-Cl16	2.3533(7)	Ru2-Cl4	2.3542(6)		
	Ru2-Cl5	2.3703(6)	Ru2-Cl6	2.3542(6)		
	Ru2-Cl6	2.3441(6)	Ru2-Cl5	2.3542(6)		
	Ru2-Cl17	2.3562(7)				
	Ru2-Cl22	2.3356(7)				
Ru-O					Ru1-O4	2.1337(11)

	Complex 2' (polymorph)		Complex 3		Complex 4	
Ru-S	Ru1-S2	2.2492(17)	Ru1-S1[2]	2.3463(8)		
	Ru1-S1	2.2701(16)	Ru1-S1[1]	2.3463(8)		
	Ru1-S3	2.2832(19)	Ru1-S1	2.3463(8)		
	Ru2-S7	2.2469(17)	Ru1-S1[3]	2.3463(8)		
	Ru2-S6	2.2749(16)				
	Ru2-S8	2.2893(18)				
Ru-Cl	Ru1-Cl2	2.4242(17)	Ru1-Cl1[1]	2.4036(11)	Ru1-Cl1	2.3292(18)
	Ru1-Cl1	2.4273(17)	Ru1-Cl1	2.4036(11)	Ru1-Cl2	2.3389(19)
	Ru2-Cl3	2.4228(17)			Ru1-Cl3	2.3575(17)
	Ru2-Cl4	2.4260(17)				
Ru-O	Ru1-O4	2.143(4)			Ru1-O1	1.7673(5)
	Ru2-O5	2.130(5)			Ru1-O2	2.055(4)
					Ru1-O3	2.1(2)

Table S4: Selected bond angles in degrees for complex **1** at 100K and 250 K, and polymorph **2'**. Atoms are labelled in **Figure S4** for clarity.

	Complex 1 (100 K)		Complex 1 (250 K)		Complex 2' (polymorph)	
S-Ru-Cl	S1-Ru1-Cl3	89.19(2)	S1-Ru1-Cl1	89.261(15)	S7-Ru2-Cl4	88.92(6)
	S1-Ru1-Cl4	90.76(3)	S1-Ru1-Cl1	89.261(15)	S6-Ru2-Cl4	91.12(6)
	S1-Ru1-Cl15	88.05(2)	S1-Ru1-Cl3	90.739(15)	S8-Ru2-Cl4	175.85(7)
	S1-Ru1-Cl16	91.69(2)	S1-Ru1-Cl3	90.739(15)	S2-Ru1-Cl1	89.96(6)
	S2-Ru1-Cl3	89.08(2)	S1-Ru1-Cl2	88.09(2)	S1-Ru1-Cl1	91.29(6)
	S2-Ru1-Cl4	90.97(3)	S1-Ru1-Cl2	91.92(2)	S3-Ru1-Cl1	175.11(7)
	S2-Ru1-Cl15	91.92(2)	S1-Ru1-Cl2	91.92(2)	S7-Ru2-Cl3	89.28(6)
	S2-Ru1-Cl16	88.36(2)	S1-Ru1-Cl2	88.09(2)	S6-Ru2-Cl3	173.07(7)
	S3-Ru2-Cl5	87.60(2)	S2-Ru2-Cl5	87.66(9)	S8-Ru2-Cl3	89.50(6)
	S3-Ru2-Cl6	92.03(2)	S2-Ru2-Cl5	92.33(9)	S2-Ru1-Cl2	88.69(6)
	S4-Ru2-Cl5	92.36(2)	S2-Ru2-Cl4	90.020(14)	S1-Ru1-Cl2	173.67(6)
	S4-Ru2-Cl6	88.01(2)	S2-Ru2-Cl4	90.020(14)	S3-Ru1-Cl2	89.17(6)
	S3-Ru2-Cl22	91.34(3)	S2-Ru2-Cl5	87.66(9)		
	S4-Ru2-Cl22	88.19(3)	S2-Ru2-Cl5	92.33(9)		
	S3-Ru2-Cl17	89.05(2)	S2-Ru2-Cl6	89.980(14)		
	S4-Ru2-Cl17	91.41(2)	S2-Ru2-Cl16	89.980(14)		
S-Ru-S	S2-Ru1-S1	178.27(2)	S2-Ru2-S2	179.96(3)	S7-Ru2-S6	97.64(7)
	S4-Ru2-S3	179.53(2)	S1-Ru1-S1	178.52(3)	S2-Ru1-S3	94.37(7)
					S1-Ru1-S3	90.39(6)
					S2-Ru1-S1	97.64(6)
					S7-Ru2-S8	94.75(6)
					S6-Ru2-S8	90.30(6)
Cl-Ru-Cl	Cl4-Ru1-Cl3	179.52(3)	Cl1-Ru1-Cl3	180	Cl2-Ru1-Cl1	88.66(6)
	Cl15-Ru1-Cl3	90.94(3)	Cl1-Ru1-Cl2	90.377(19)	Cl3-Ru2-Cl4	88.61(6)
	Cl15-Ru1-Cl4	89.53(3)	Cl3-Ru1-Cl2	89.623(19)		
	Cl16-Ru1-Cl3	90.10(3)	Cl1-Ru1-Cl2	90.378(19)		
	Cl16-Ru1-Cl4	89.42(3)	Cl3-Ru1-Cl2	89.622(19)		
	Cl16-Ru1-Cl15	178.92(2)	Cl2-Ru1-Cl2	179.24(4)		
	Cl6-Ru2-Cl5	179.28(3)	Cl5-Ru2-Cl4	101.71(18)		
	Cl17-Ru2-Cl5	88.90(3)	Cl5-Ru2-Cl4	101.71(18)		
	Cl17-Ru2-Cl6	90.47(3)	Cl6-Ru2-Cl5	78.29(18)		
	Cl22-Ru2-Cl5	89.04(3)	Cl6-Ru2-Cl4	180		
	Cl22-Ru2-Cl6	91.58(3)	Cl6-Ru2-Cl5	78.29(18)		
	Cl22-Ru2-Cl17	177.89(3)	Cl5-Ru2-Cl5	156.6(4)		
O-Ru-S					O4-Ru1-S2	175.07(14)
					O4-Ru1-S1	86.19(13)
					O4-Ru1-S3	88.69(15)
					O5-Ru2-S7	174.89(14)
					O5-Ru2-S6	85.66(13)
					O5-Ru2-S8	89.12(15)
O-Ru-Cl					O4-Ru1-Cl2	87.48(13)
					O4-Ru1-Cl1	86.83(15)
					O5-Ru2-Cl4	87.11(15)
					O5-Ru2-Cl3	87.42(13)

Table S5. Selected bond angles in degrees for complexes **2-4**. Atoms are labelled in **Figure S4** for clarity.

	Complex 2		Complex 3		Complex 4	
S-Ru-Cl	S2-Ru1-Cl6	94.727(14)	S1-Ru1-Cl1	90		
	S2-Ru1-Cl15	89.699(14)	$S1^{3}$-Ru1-$Cl1^{1}$	90		
	S7-Ru1-Cl15	172.750(14)	$S1^{2}$-Ru1-$Cl1^{1}$	90		
	S16-Ru1-Cl6	171.813(14)	$S1^{1}$-Ru1-Cl1	90		
	S7-Ru1-Cl6	87.245(14)	$S1^{3}$-Ru1-Cl1	90		
	S16-Ru1-Cl5	92.017(14)				
S-Ru-S	S2-Ru1-S16	93.259(14)	S1-Ru1-$S1^{2}$	90		
	S7-Ru1-S16	93.996(14)	S1-Ru1-$S1^{1}$	180		
	S2-Ru1-S7	93.995(15)	$S1^{1}$-Ru1-$S1^{2}$	90		
			$S1^{1}$-Ru1-$S1^{3}$	90		
			S1-Ru1-$S1^{3}$	90		
Cl-Ru-Cl	Cl15-Ru1-Cl6	86.235(14)			Cl1-Ru1-Cl2	89.76(7)
					Cl1-Ru1-Cl3	91.53(7)
					Cl2-Ru1-Cl3	172.07(6)
O-Ru-Cl	O12-Ru1-Cl6	87.04(3)			O1-Ru1-Cl1	95.69(7)
	O12-Ru1-Cl5	89.33(3)			O2-Ru1-Cl1	171.72(13)
					O3-Ru1-Cl1	89(7)
					O1-Ru1-Cl2	93.70(19)
					O2-Ru1-Cl2	85.40(13)
					O3-Ru1-Cl2	87(7)
					O1-Ru1-Cl3	93.95(18)
					O2-Ru1-Cl3	92.36(13)
					O3-Ru1-Cl3	85(7)
O-Ru-S	O12-Ru1-S2	177.92(3)				
	O12-Ru1-S7	87.17(3)				
	O12-Ru1-S16	84.94(3)				
O-Ru-O					O1-Ru1-O2	91.33(13)
					O1-Ru1-O3	175(7)
					O2-Ru1-O3	84(7)
Ru-O-Ru					Ru1-O1-$Ru1^{2}$	178.4(4)

Table S6: Differences in the unit cell parameters in previously reported monoclinic and orthorhombic forms of complex **2.**

	Space Group	*a* (Å)	*b* (Å)	*c* (Å)	*β* (°)	CSD Code
Monoclinic I	$P2_1/c$	8.939(3)	18.045(7)	11.363(3)	91.52(2)	*CDMSOR*[11] *CDMSOR04*[12] *CDMSOR06* *CDMSOR08* *CDMSOR09*
Monoclinic II	$P2_1/n$	8.417(2)	27.695(4)	8.598(2)	116.88(3)	*CDMSOR02*[13]
Monoclinic III	$P2_1/c$	10.1479(3)	10.4626(3)	18.4280(4)	99.795(14)	*CDMSOR0*[14]
Monoclinic IV	$P2_1$	8.3145(9)	27.629(3)	8.542(1)	117.039(3)	*CDMSOR10*
Orthorhombic	*Pccn*	28.328(5)	10.831(3)	11.751(3)		*CDMSOR01*[15] *CDMSOR03*[16] *CDMSOR07* *CDMSOR11*

Table S7: TD-DFT calculated UV-vis spectra peaks, extinction coefficients and their transition type.

	λ (nm)	Extinction coefficient	Transition type
$[(Ru(IV)Cl_3(DMSO)_2)_2(\mu\text{-}O)]$ 4	536	2830	d-d, LUMO ($d_{x^2-y^2} + O_{px}$) ← Cl_p, d_{xy}
	566	0.0038	LM, ($d_{x^2-y^2} + O_{px}$) ← Cl
$[(Ru(IV)Cl_3(DMSO)_2)(\mu\text{-}O)(Ru(III)Cl_3(DMSO)_2)]$ Reduced 4	675	0.0011	d-d, SOMO($d_{x^2-y^2} + O_{px} + Cl$) ← Cl_p,d_{xy} d-d LUMO($d_{x^2-y^2} + O_{px} + Cl$) ← $Ru^a(d_{xz})$ + Cl
	790	420	d-d LUMO($d_{x^2-y^2} + O_{px} + Cl$) ← $Ru^a(d_{xz})$ + Cl
	877	0.001	d-d, SOMO($d_{x^2-y^2} + O_{px} + Cl$) ← $Ru^a(d_{xz})$ + Cl
$[(Ru(IV)Cl_3(MeCN)_2)_2(\mu\text{-}O)]$ 4a (DMSO replaced by MeCN)	1160	0.0001	d-d (LUMO+2) $d_{x^2-y^2} + O_{px} + Cl$ ← $d_{x^2-y^2} + Cl$
	1710	< 0.0001	d-d LUMO ($d_{x^2-y^2} + O_{px} + Cl$) ← $d_{x^2-y^2} + Cl$
$[(Ru(IV)Cl_3(MeCN)_2)(\mu\text{-}O)](Ru(III)Cl_3(MeCN)_2)$ Reduced 4a (DMSO replaced by MeCN)	833	0.0002	d-d LUMO ($d_{x^2-y^2} + O_{px} + Cl$) ← $d_{x^2-y^2} + Cl$
	1104	23	d-d LUMO ($d_{x^2-y^2} + O_{px} + Cl$) ← $d_{x^2-y^2}$+ Cl

Table S8: Observed cathodic and anodic cyclic voltammetry peaks for a 1 mM solution of complexes **1**-**4** in acetonitrile, containing 0.1 M NBu_4PF_6 as supporting electrolyte under N_2 at a scan rate of 100 mV s^{-1}, with AgCl/Ag as reference electrode.

	Anodic Peaks (V)	Cathodic Peaks (V)
Complex 1	-0.38, -0.01, 1.53, 1.16, 1.9	-0.49, -0.42, 1.10, 1,44, 1.85
Complex 2	1.21, 1.73	-0.44, 0.45, 0.99, 1.57
Complex 3	-1.07, 0.75, 1.23, 1.77	-1.31, 0.86, 1.02, 1.56
Complex 4	-1.26, 0.14, 0.99, 1.45, 1.71	-1.56, -1.20, -0.58, -0.13, 0.54

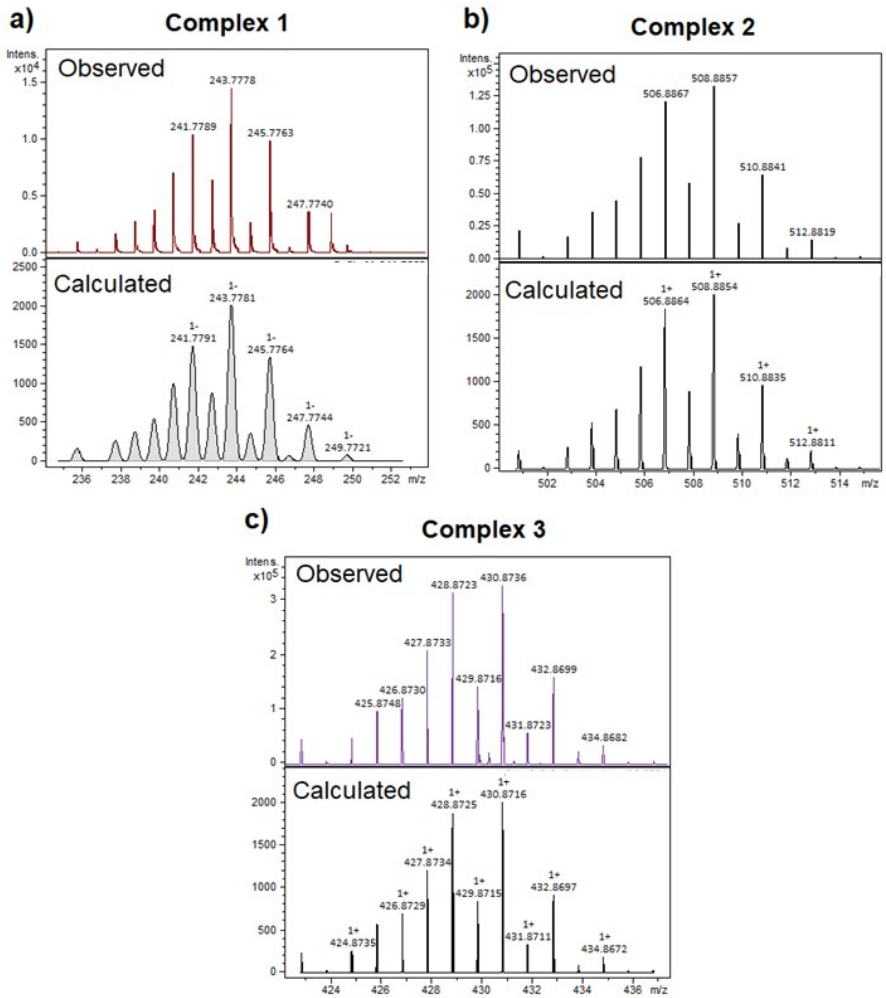

Figure S1. HRMS data for (**a**) complex **1**: Obs. 243.78, calc. for $[RuCl_4]^-$ 243.78 m/z, (**b**) complex **2**: Obs. 508.8857, calc. for $[M+Na]^+$ 508.8854 m/z, (**c**) complex **3**: Obs. 430.8736, calc. for $[M\text{-}DMSO +Na]^+$ 430.8716 m/z.

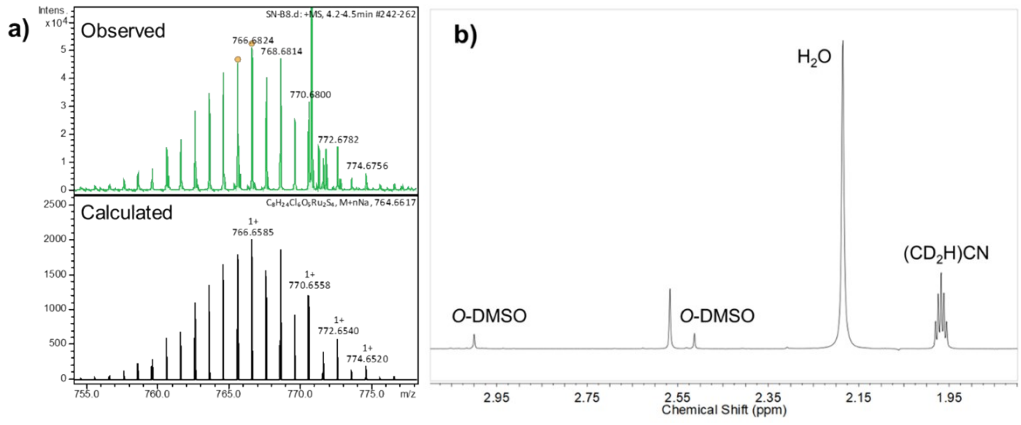

Figure S2. (**a**) HRMS data for complex **4**: Obs. 766.68, calc. for $[(Ru_2((DMSO)_2Cl_3)_2(\mu\text{-}O))+Na]^+$ = 766.66 m/z; (**b**) ^{1}H-NMR (500 MHz, CD_3CN) spectrum of complex **4.**

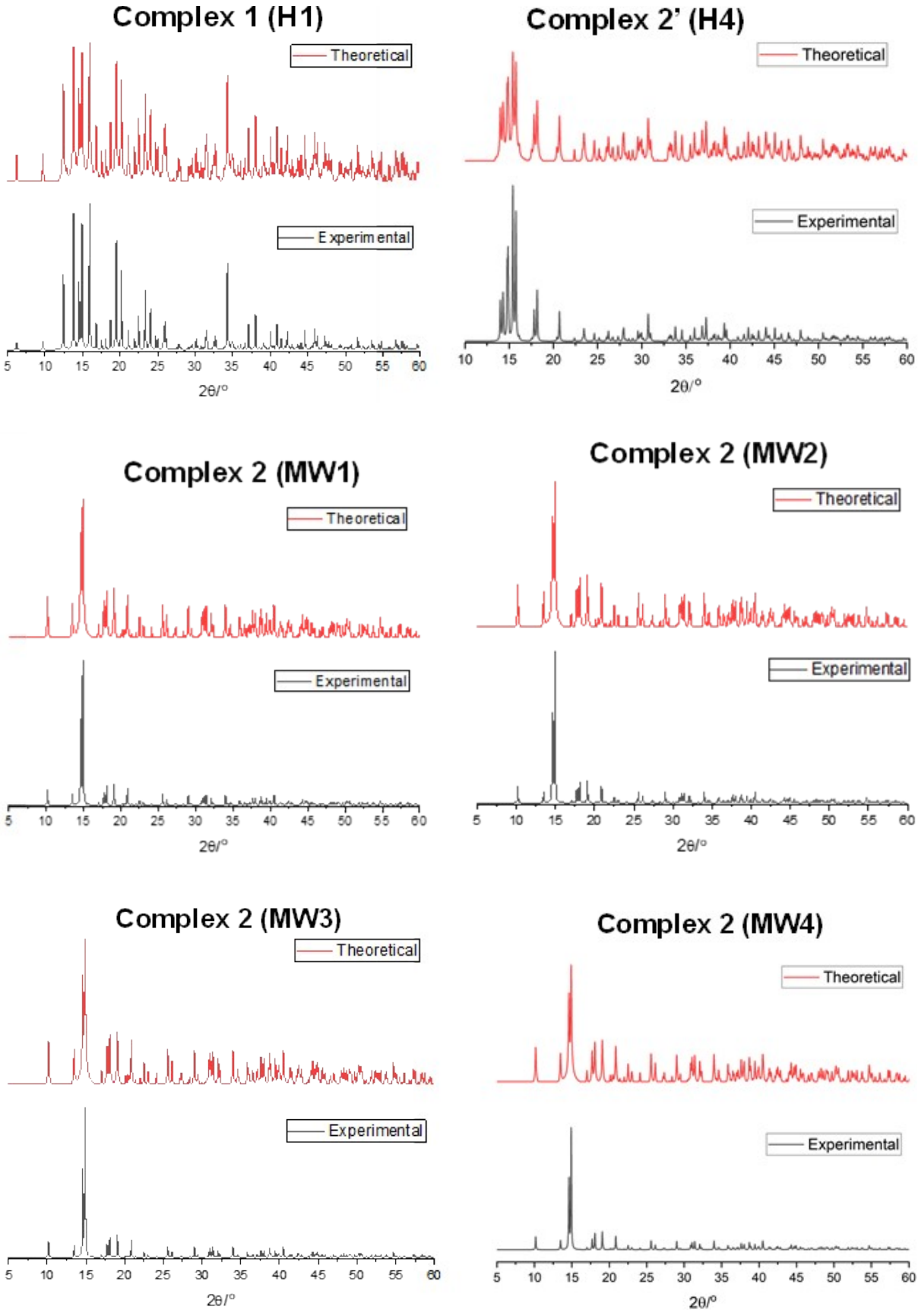

Figure S3. Comparison between experimental (black) and theoretical (red) PXRD patterns of complexes **1** obtained through ***H1*** method, complex **2'** obtained through the ***H4*** method, complex **2** obtained through the ***MW1-MW4*** methods, complex **3** obtained through the ***MW5*** method and complex **4** obtained through ***S1*** method. The theoretical powder diffraction data were simulated in Mercury from SCXRD data. PXRD patterns show good correspondence between experimental and simulated data, confirming that the bulk material is consistent with the single-crystal structure.

a)

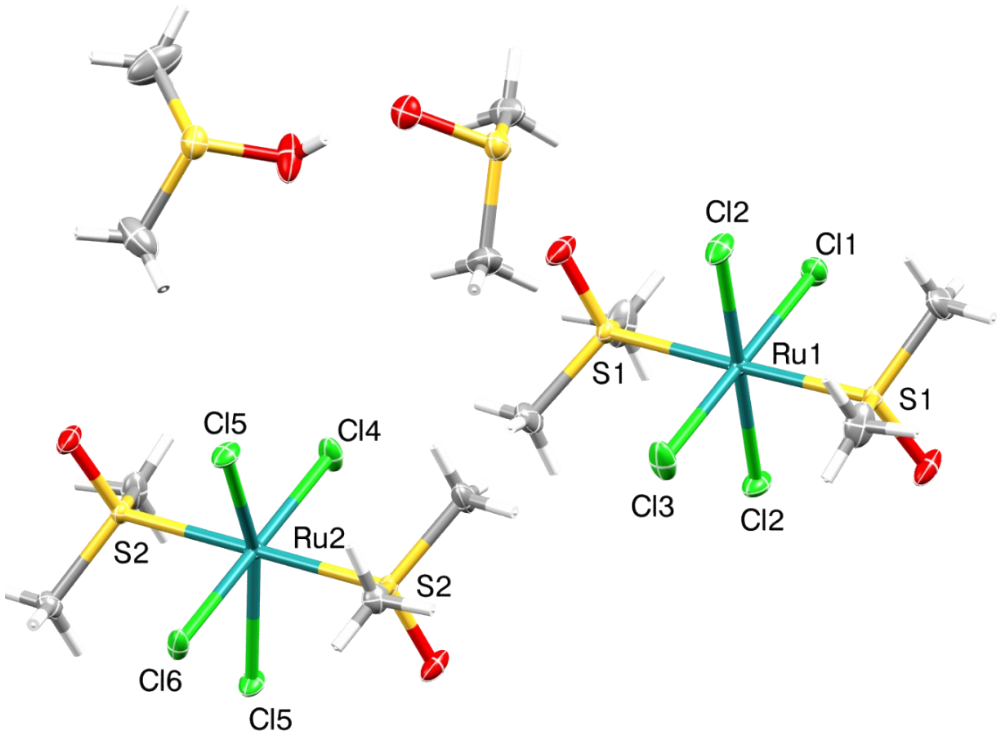
Cl2
Cl1
Ru1
S1
S1
Cl3
Cl2
Cl5
Cl4
S2
Ru2
S2
Cl6
Cl5

b)

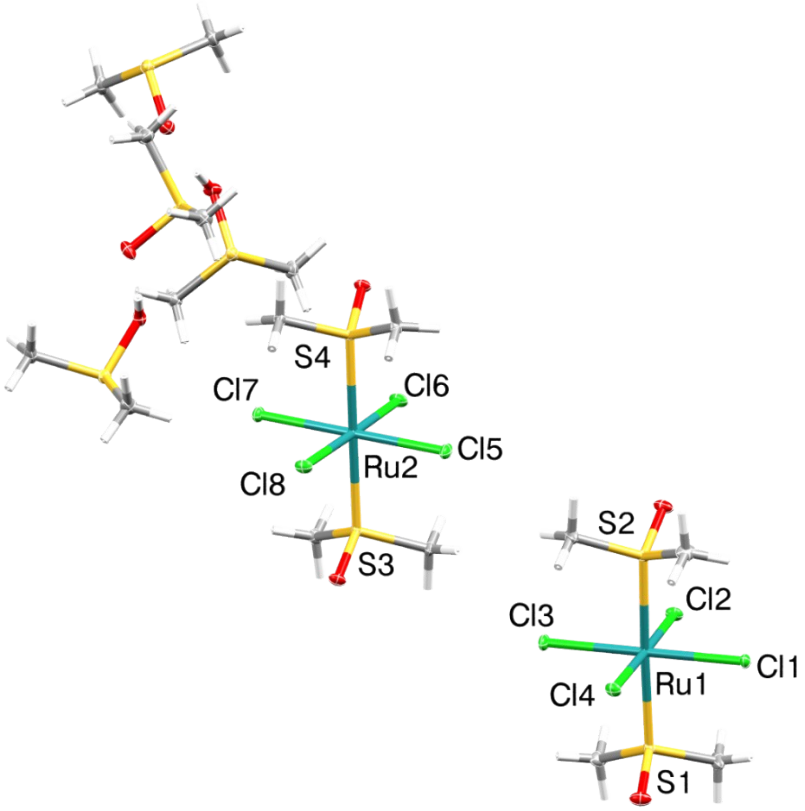
S4
Cl7
Cl6
Cl5
Ru2
Cl8
S3
S2
Cl2
Cl3
Cl1
Cl4
Ru1
S1

c)

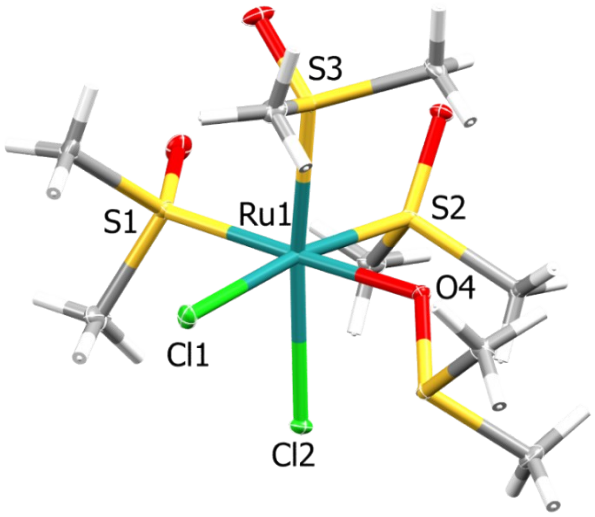
S3
S1
Ru1
S2
O4
Cl1
Cl2

d)

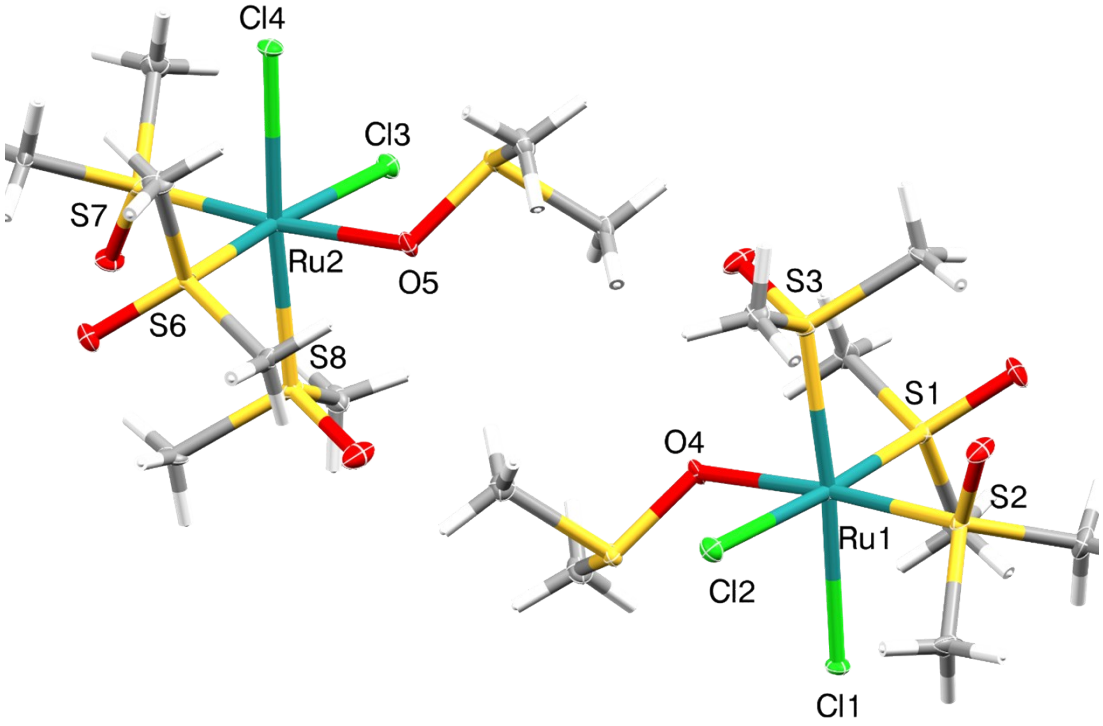
Cl4
Cl3
S7
Ru2
O5
S6
S8
S3
S1
O4
S2
Ru1
Cl2
Cl1

e)

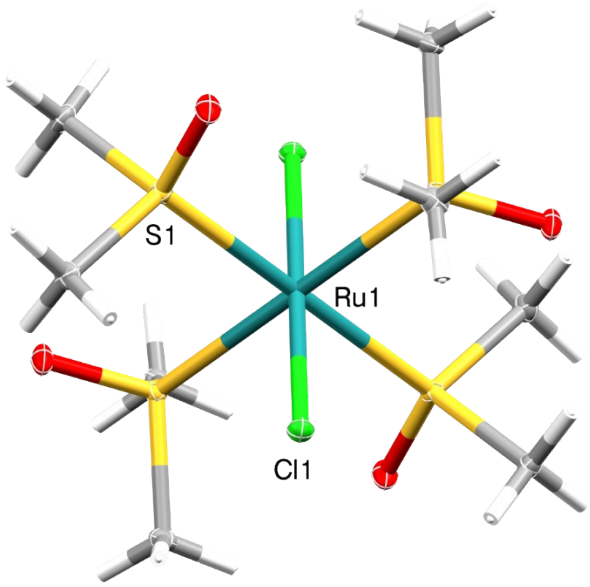

f)

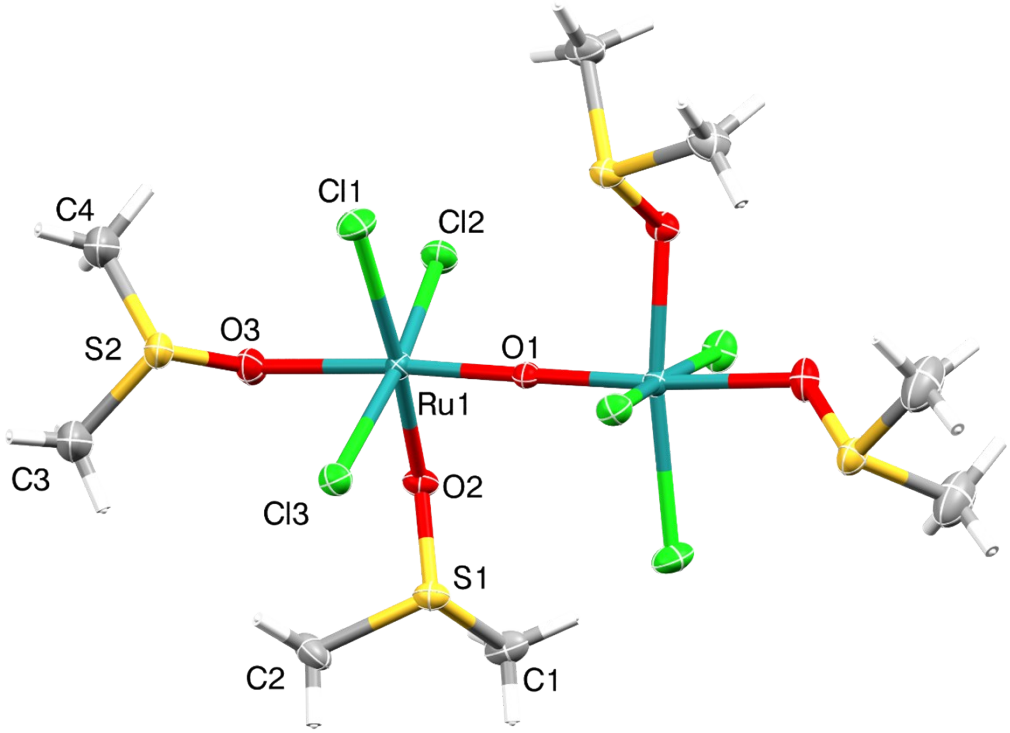

Figure S4. Crystal structures of the complexes **1-4** with ellipsoid atoms drawn at 30% of thermal probability. (**a**) Complex **1** (250 K), (**b**) complex **1** (100 K), (**c**) complex **2**, (**d**) complex **2'** (polymorph), (**e**) complex **3** and (**f**) complex **4.** Atoms are labelled as follows: Ru (blue), S (yellow), Cl (green), O (red), C (grey) and H (white) atoms. Symmetry code for complex **4** i = 1-x, ½-y, -z.

a)

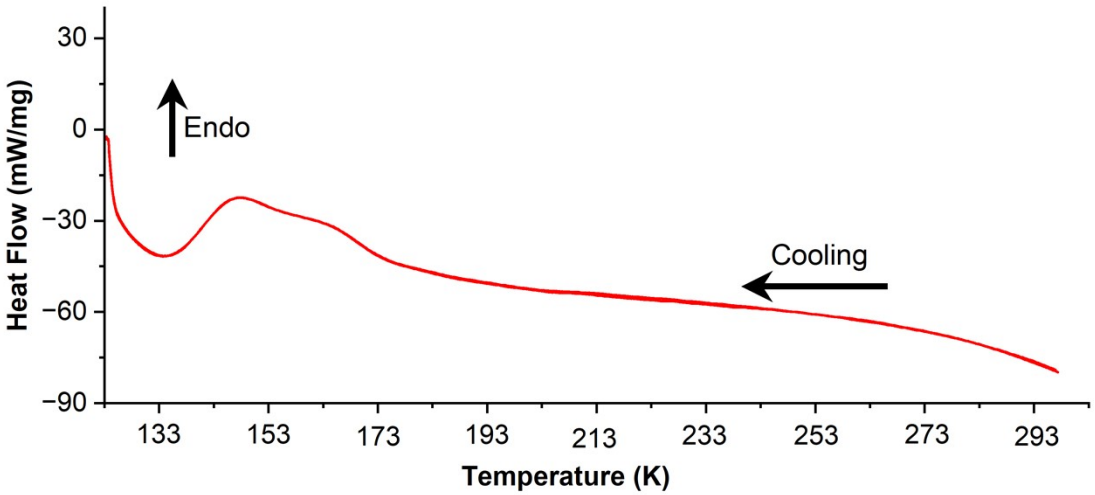
30
0
−30
−60
−90
Heat Flow (mW/mg)
Endo
Cooling
133
153
173
193
213
233
253
273
293
Temperature (K)

b)

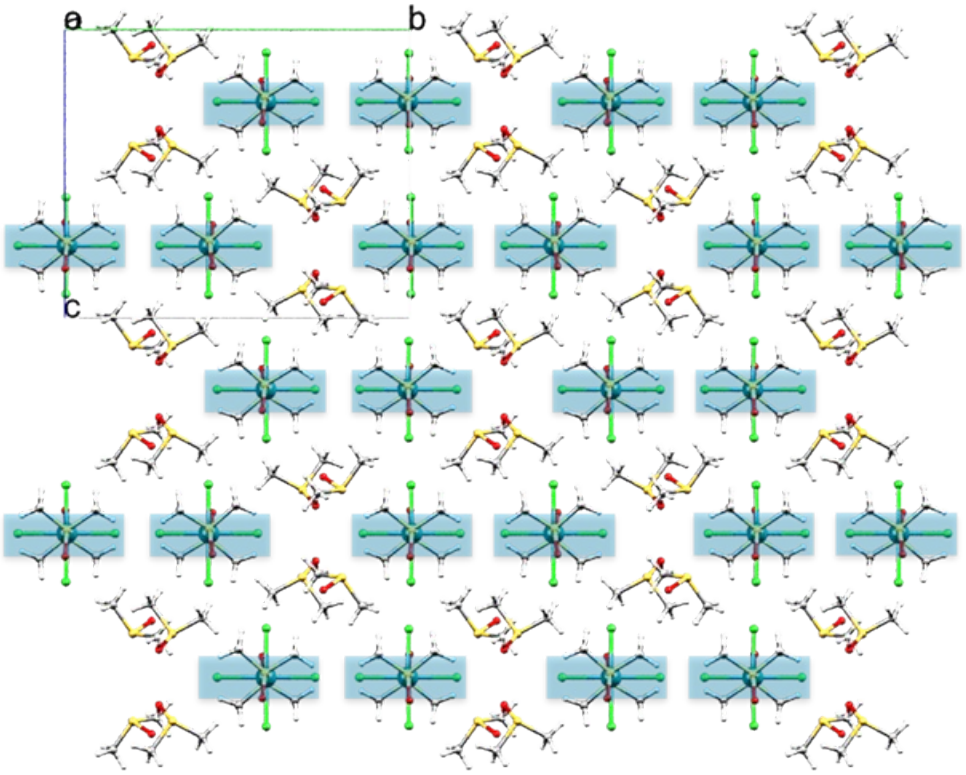
a
b
c

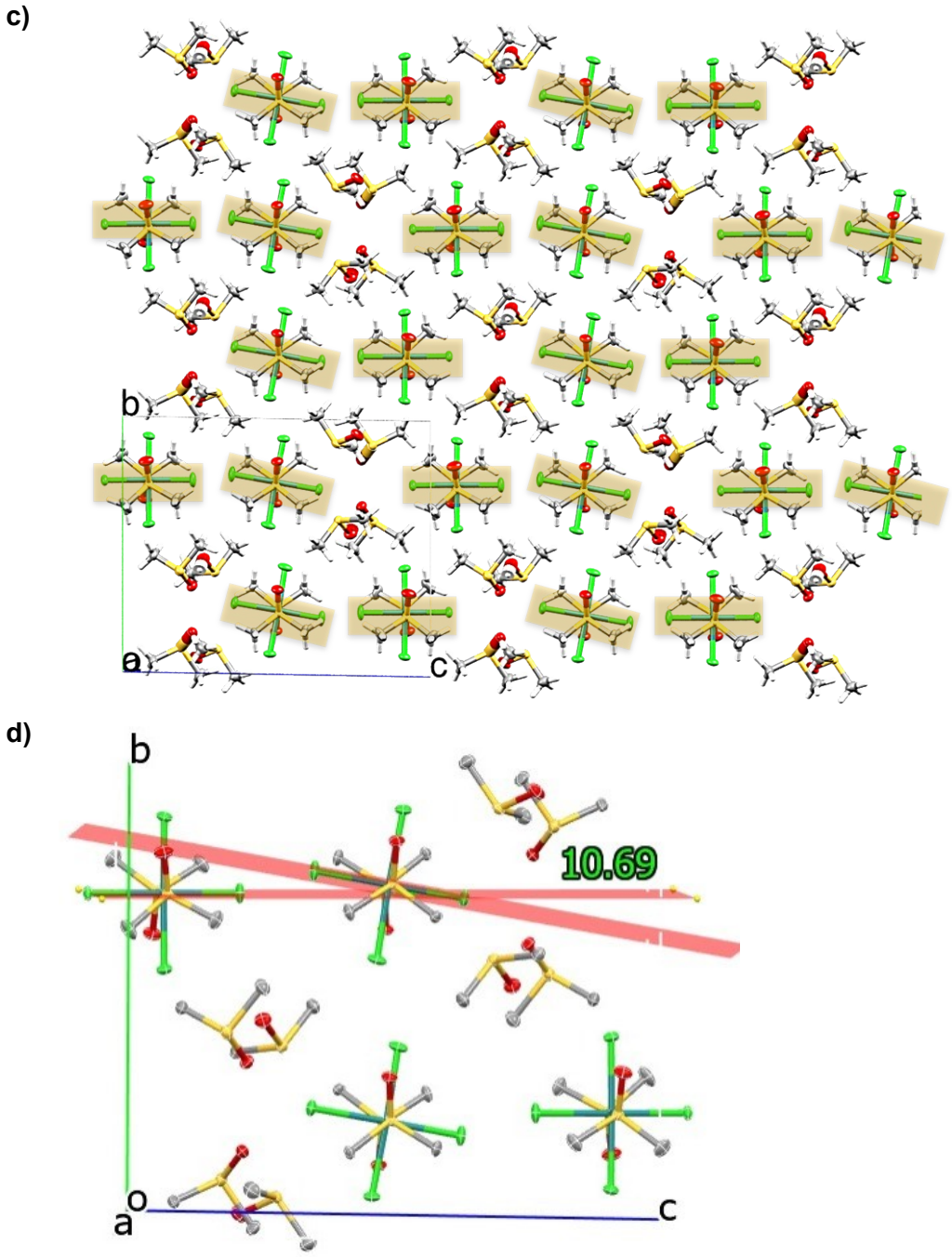

Figure S5. (**a**) Differential scanning calorimetry (DSC) of **1**, confirming a phase transition in the range of 163-133 K. Crystal packing views of complex **1** (**b**) along *a*-axis at 298 K, (**c**) and at 100 K. (**d**) The structure at 100 K; the molecules are twisted by 10.69° relative to Cl-Ru-Cl axes.

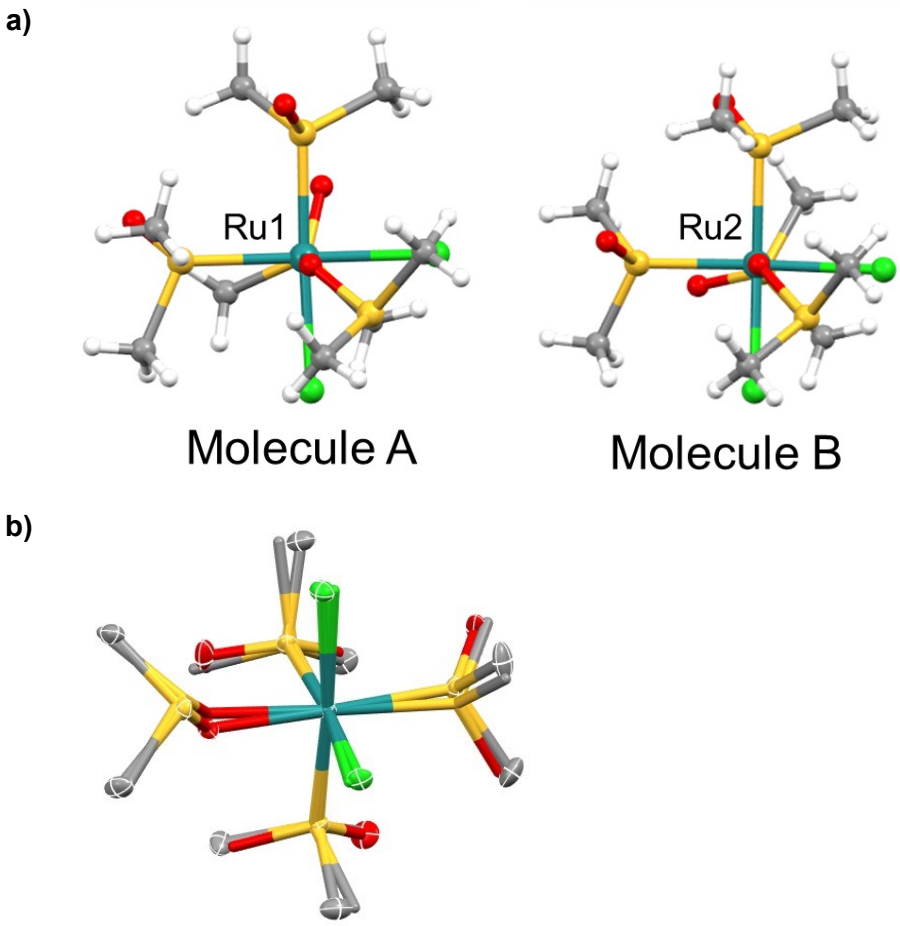

Figure S6. (**a**) Perspective view showing the conformational difference between the two molecules A and B present in the asymmetric unit of polymorph **2'**. (**b**) Overlapped view of molecules A and B, showing the difference in the conformation of the *S*-bounded DMSO ligands.

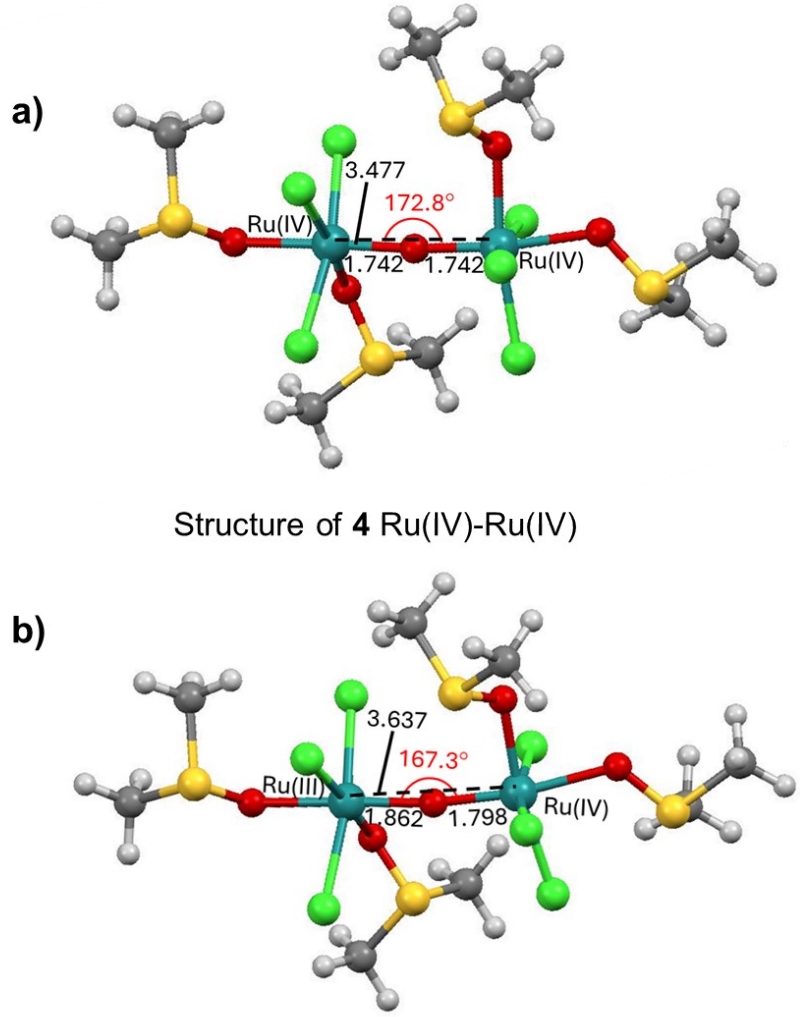

Figure S7. DFT-calculated structures of (**a**) **4** Ru(IV)-(IV), and (**b**) one-electron-reduced **4** Ru(III)-(IV). Bond distances (black) are in Å. Bond angles (red) are in degrees. The simulated structure of **4** is in good agreement with data from SCXRD calculations.

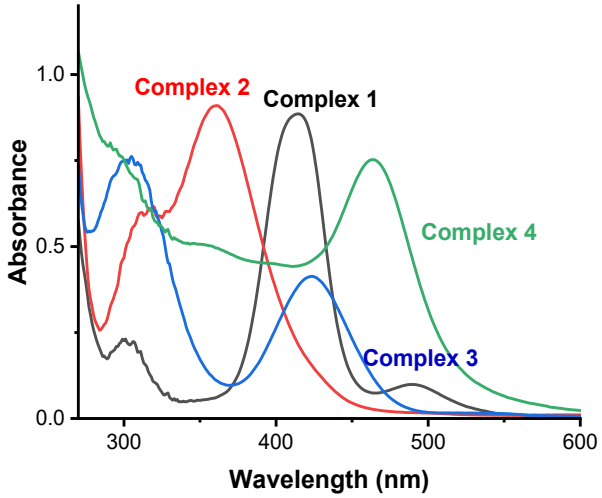

Figure S8. UV-vis spectra of complexes **1-4** in acetonitrile.

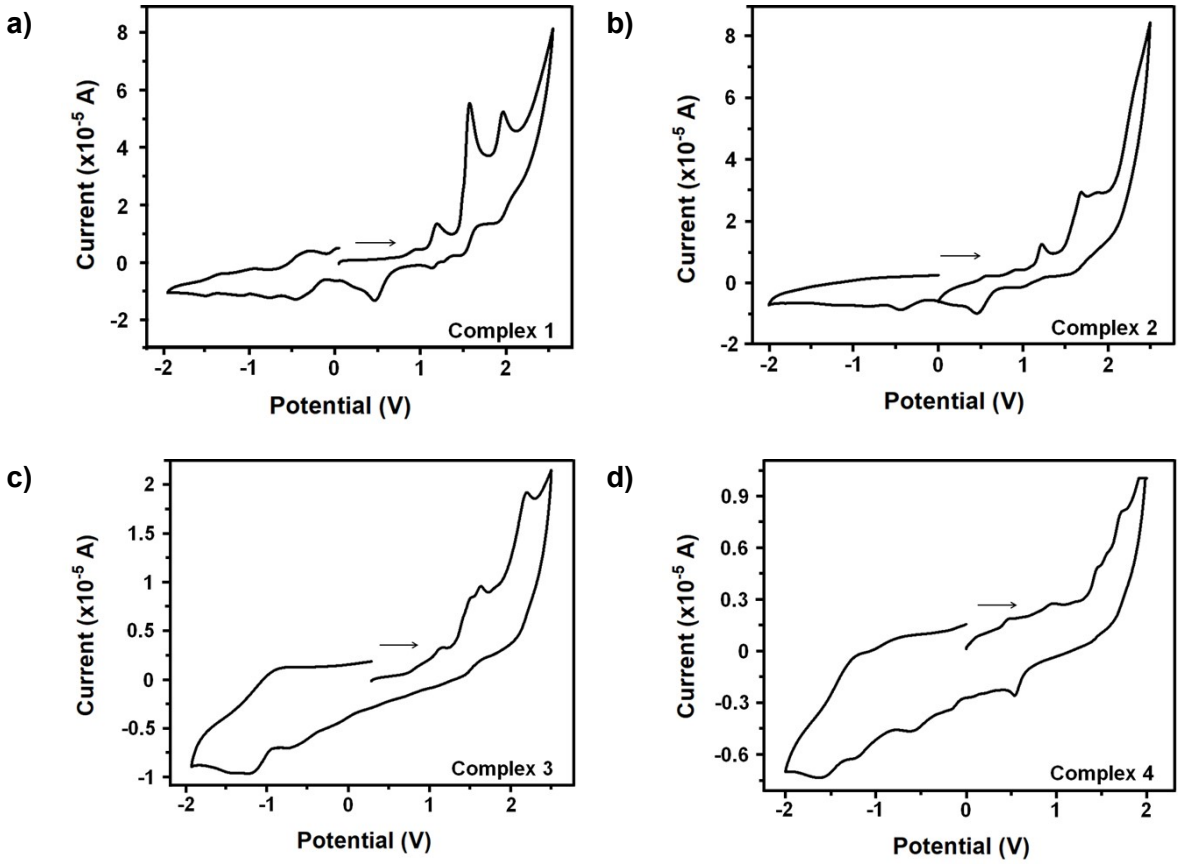

Figure S9. Cyclic voltammograms of 1 mM solutions in acetonitrile of (**a**) complex **1**, (**b**) complex **2**, (**c**) complex **3** and (**d**) complex **4**, containing 0.1 M NBu_4PF_6 as supporting electrolyte under N_2 at a scan rate of 100 mV s^{-1}, with AgCl/Ag as reference electrode.

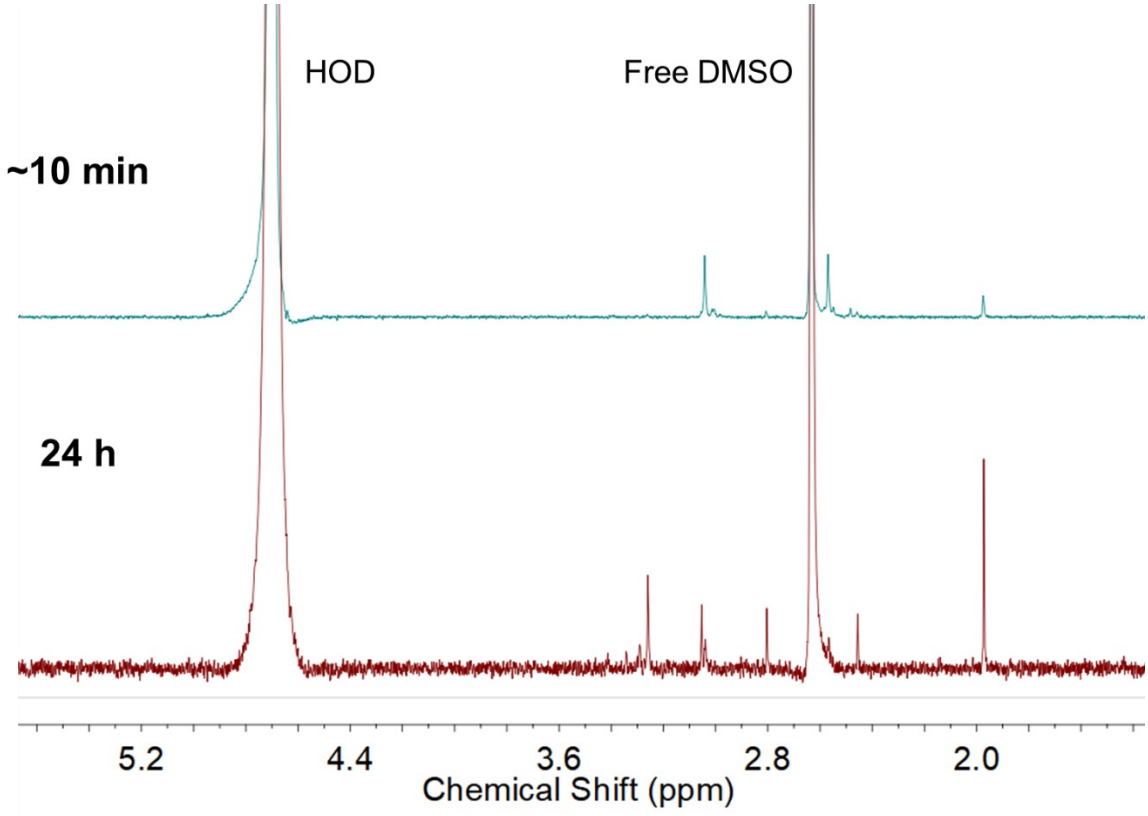

Figure S10. 400 MHz ^{1}H-NMR spectrum of complex **4** in D_2O (10 mM). 10 min (top, blue) and 24 h (bottom, red) after dissolution at 293 K.

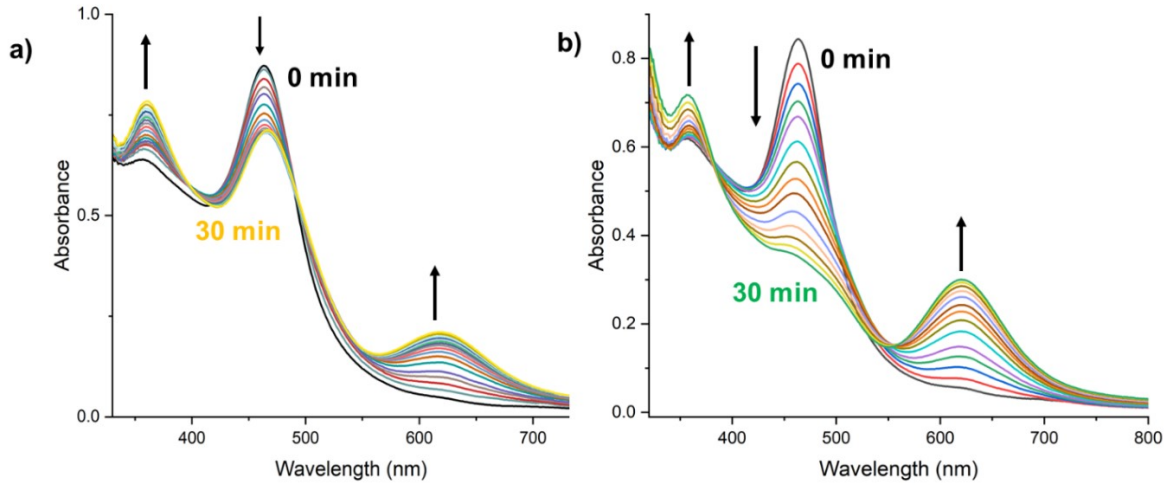

Figure S11. UV-vis spectra of complex **4** (0.1 mM) on reaction with (**a**) 0.5 mol equiv and (**b**) 2 mol equiv ferrocene in acetonitrile, monitored every minute over a period of 30 min.

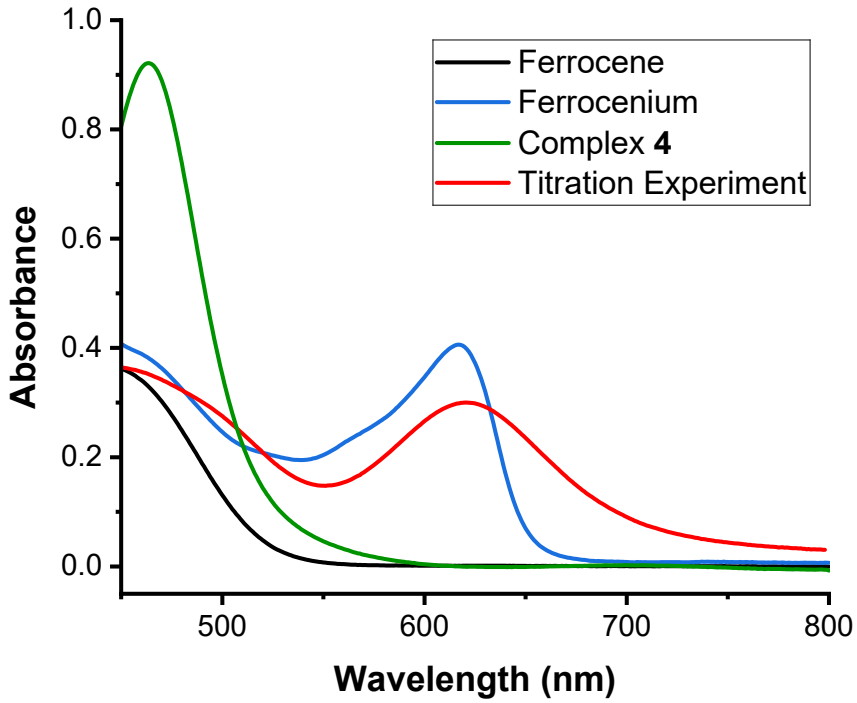

Figure S12: UV-vis spectra in the region between 450 nm to 800 nm of ferrocene (Fc, black), ferrocenium (blue), complex **4** (green) in comparison to the final UV-vis spectrum from the reaction between complex **4** and Fc (red). Differences in absorption around the band centred at 600 nm formed during the reaction between **4** and ferrocene are notable.

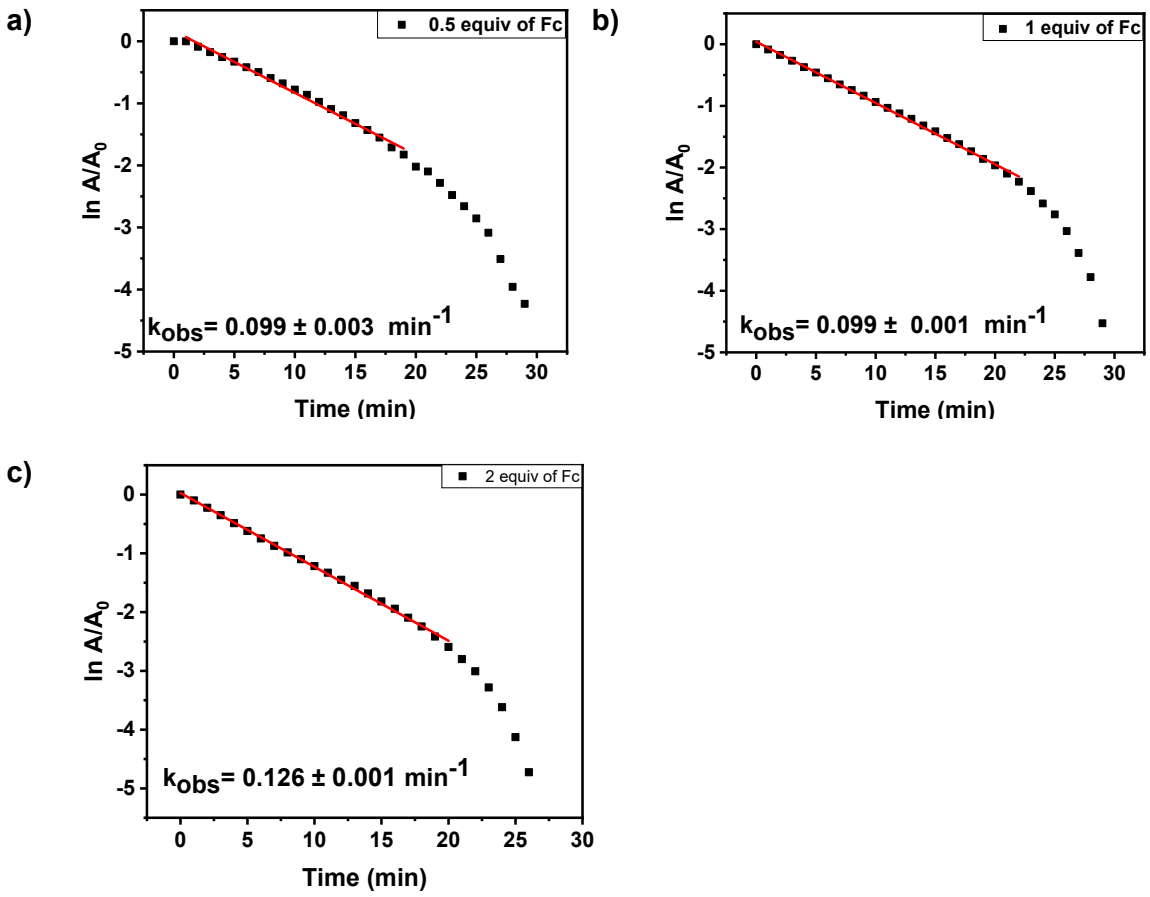

Figure S13: Plots of ln (A/A_0) vs time for the reaction between **4** and (**a)** 0.5, (**b**) 1 and (**c**) 2 mol equiv of Fc with the best fit to first-order kinetics for the early times of the reaction (red line).

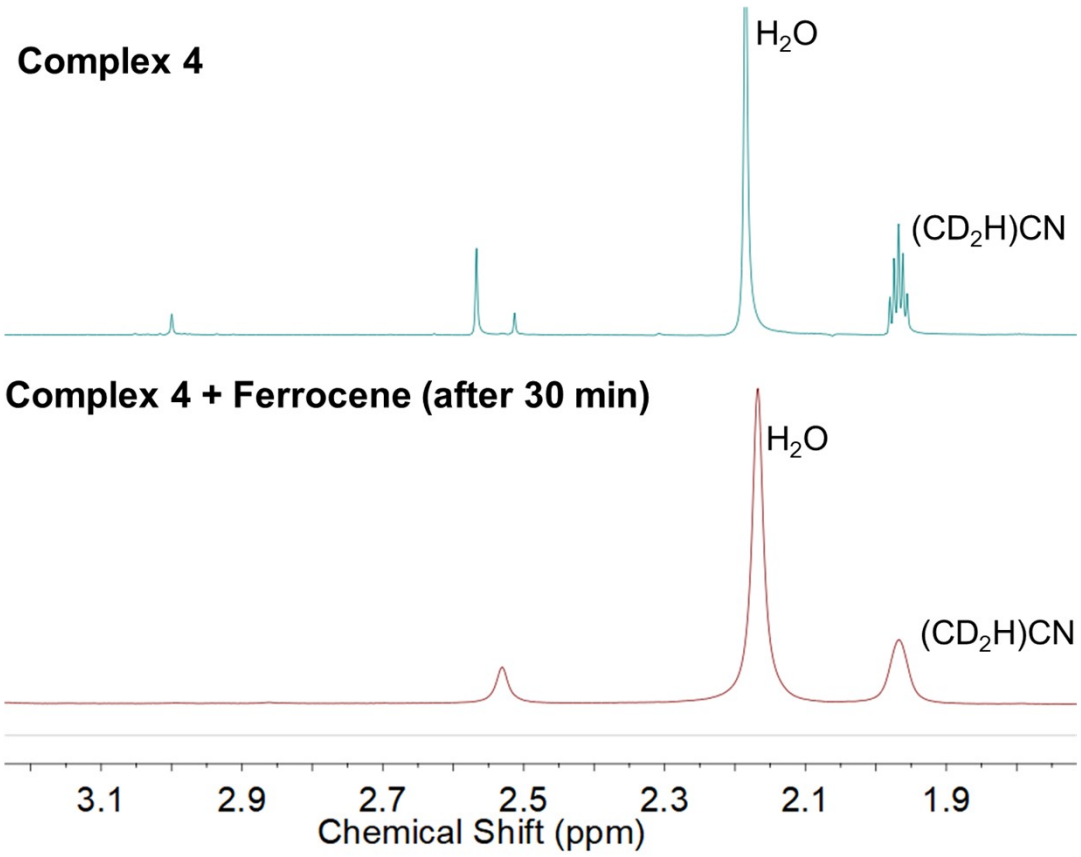

Figure S14. Comparison between ^{1}H NMR spectra (500 MHz, acetonitrile-d_3) of 10 mM complex **4** before (top, blue) and 30 min (bottom, red) after the addition of 2 mol equiv ferrocene. The solvent peaks are broadened and the Ru-DMSO peaks disappear, suggesting the formation of paramagnetic species in solution.

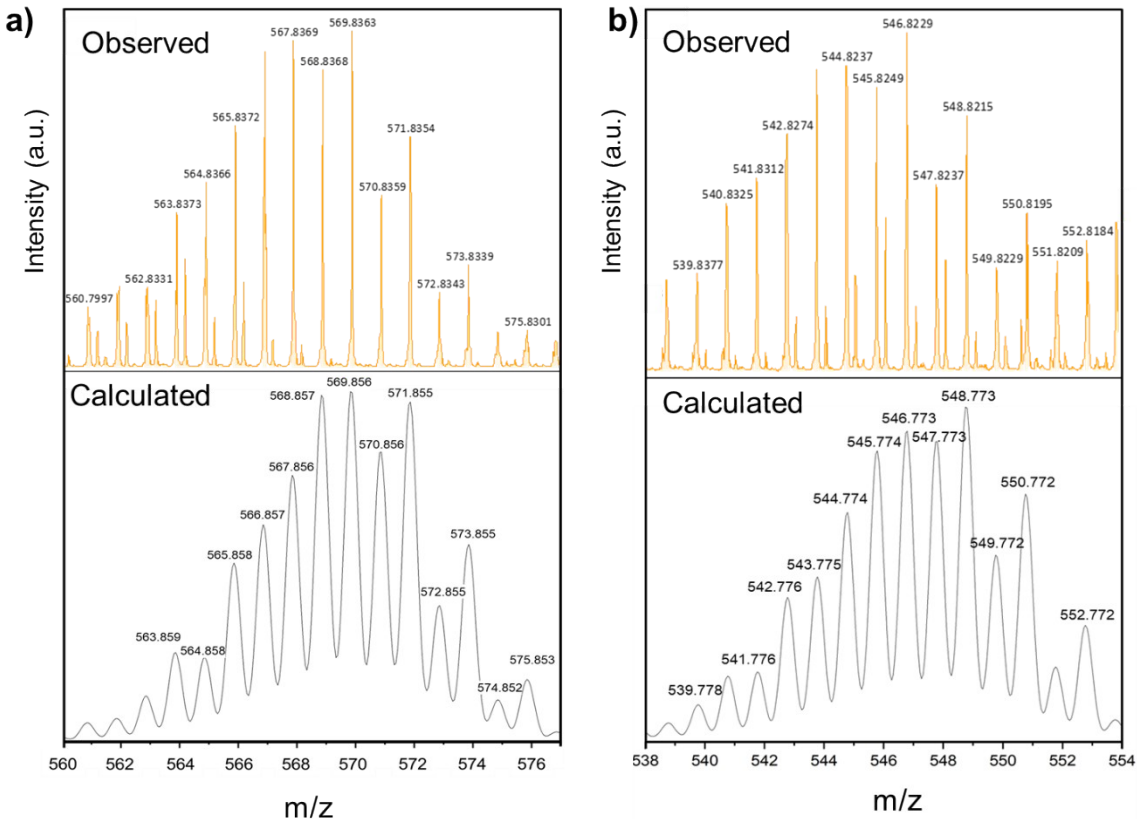

Figure S15. Positive-ion HRMS for the product obtained from reaction between complex **4** and ferrocene (1 mol equiv) in acetonitrile after 15 min of reaction. (**a)** The isotope pattern corresponds to $[Ru_2(\mu\text{-}O)(DMSO)_2Cl_2(MeCN)_3 + H]^+$ species, and (**b**) to $[Ru_2(\mu\text{-}O)Cl_4(MeCN)_4 + Na]^+$ species. The detection of these two di-Ru species suggests that the oxo-bridge is retained in the reaction.

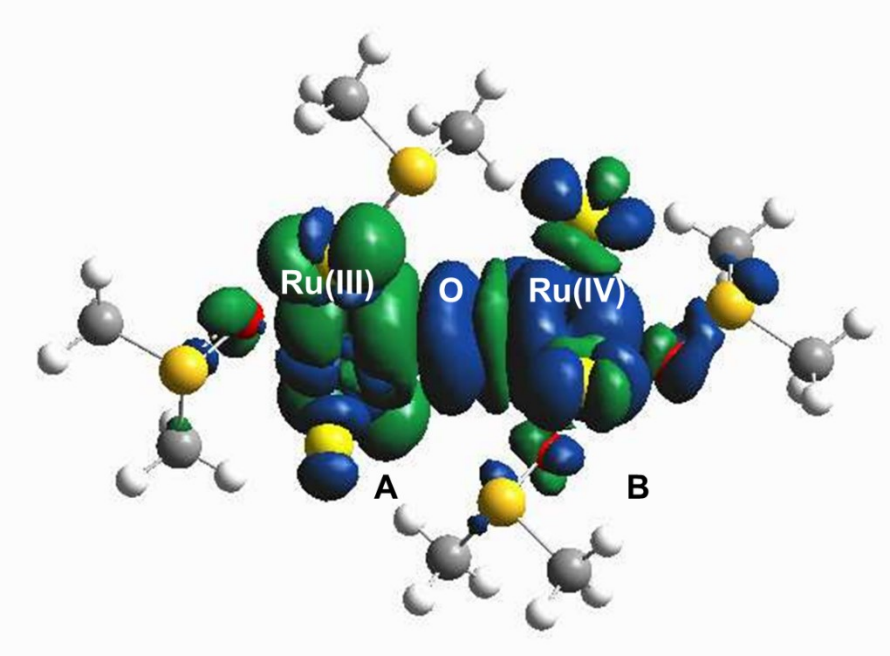

Figure S16. Calculated spin density for **4-red**(Ru(III/IV)**, the** one-electron reduced form of **4** (Ru(IV/IV)). A indicates the longer Ru(III)-O bond) and B the shorter Ru(IV)-O bond. Alpha spin density is coloured blue and beta spin density green.

References

1 E. Alessio, G. Balducci, M. Calligaris, G. Costa, W. M. Attia and G. Mestroni, *Inorg. Chem.*, 1991, **30**, 609.

2 Oxford Diffraction. CrysAlisPro Software System; Rigaku Corporation: Oxford, UK, 2015.

3 G. M. Sheldrick, *Acta Cryst. A*, 2015, **71**, 3.

4 C. F. Macrae, I. Sovago, S. J. Cottrell, P. T. A. Galek, P. McCabe, E. Pidcock, M. Platings, G. P. Shields, J. S. Stevens, M. Towler and P. A. Wood, *J. Appl. Cryst.*, 2020, **53**, 226.

5 A. D. Becke, *J. Chem. Phys*, 1993, **98**, 5648.

6 F. Weigend, *Phys. Chem. Chem. Phys.*, 2006, **8**, 1057.

7 S. Grimme, J. Antony, S. Ehrlich and H. Krieg, *J. Chem. Phys.*, 2010, **132**, 154104.

8 E. Alessio, *Chem. Rev.*, 2004, **104**, 4203.

9 I. Bratsos and E. Alessio, in *Inorganic Syntheses*, ed. T. B. Rauchfuss, John Wiley & Sons, 2010, Chapter 8, 148.

10 M. de Torres, S. Semin, I. Razdolski, J. Xu, J. A. A. W. Elemans, T. Rasing, A. E. Rowan and R. J. M. Nolte, *Chem. Commun.*, 2015, **51**, 2855.

11 A. Mercer and J. Trotter, *J. Chem. Soc., Dalton Trans.*, 1975, 2480.

12 F. C. Pigge, J. J. Coniglio and N. P. Rath, *Organometallics*, 2005, **24**, 5424.

13 E. Alessio, G. Mestroni, G. Nardin, W. M. Attia, M. Calligaris, G. Sava and S. Zorzet, *Inorg. Chem.*, 1988, **27**, 4099.

14 G. Georgieva, G. Gencheva, B. L. Shivachev and R. P. Nikolova, *Acta Cryst. E*, 2008, **64**, m1023.

15 W. M. Attia and M. Calligaris, *Acta Cryst. C*, 1987, **43**, m1426.

16 R. S. Srivastava and F. R. Fronczek, *Acta Cryst. E*, 2003, **59**, m427.